SF1

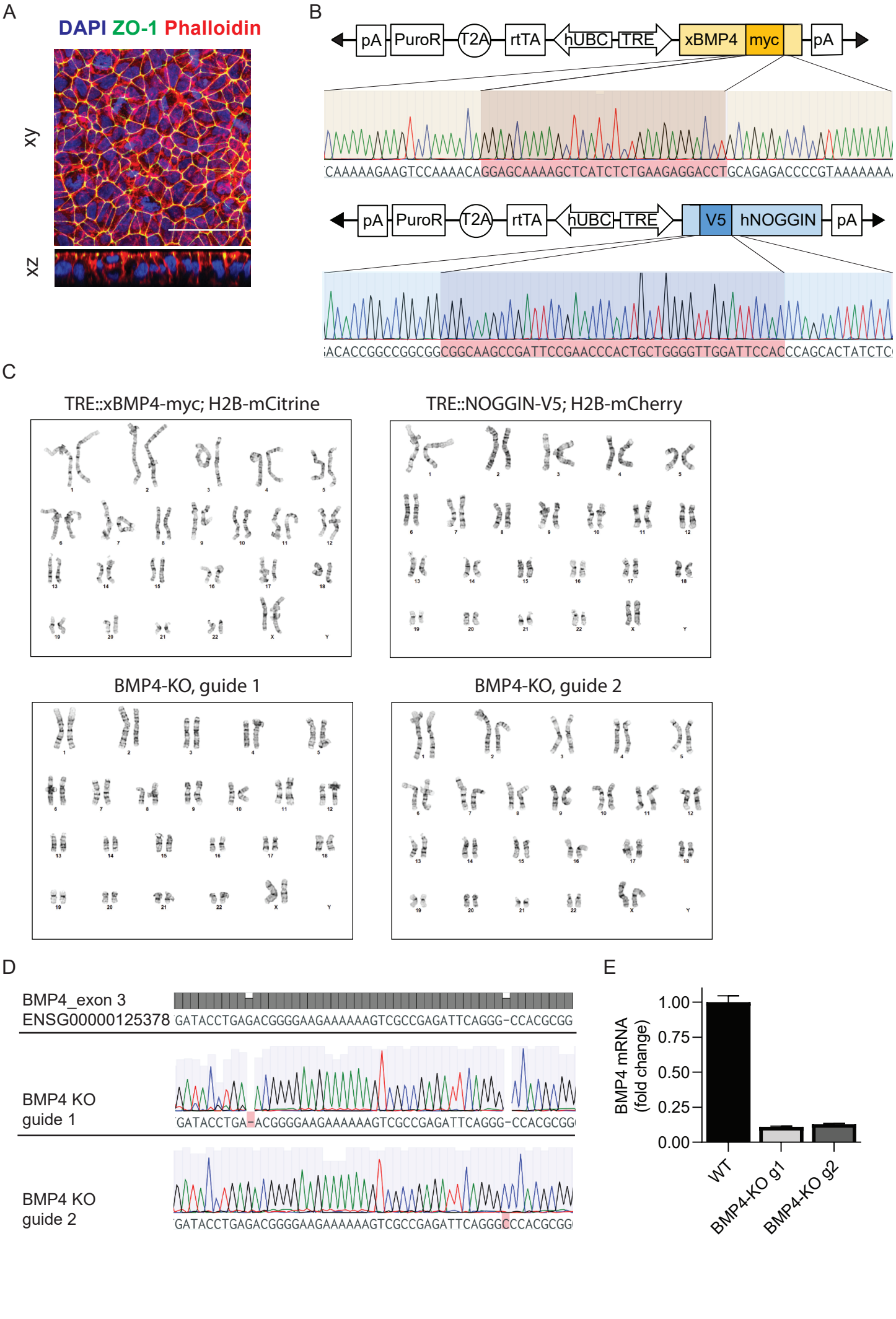
A
DAPI ZO-1 Phalloidin
xy
xz
B
pA
PuroR
T2A
rtTA
hUBC
TRE
xBMP4
myc
pA
CAAAAAGAAGTCCAAAACAGGAGCAAAAGCTCATCTCTGAAGAGGACCTGCAGAGACCCCGTAAAAAAA
pA
PuroR
T2A
rtTA
hUBC
TRE
V5
hNOGGIN
pA
ACACCGGCCGGCGGCGGCAAGCCGATTCCGAACCCACTGCTGGGGTTGGATTCCACCCAGCACTATCTC
C
TRE::xBMP4-myc; H2B-mCitrine
TRE::NOGGIN-V5; H2B-mCherry
BMP4-KO, guide 1
BMP4-KO, guide 2
D
BMP4_exon 3
ENSG00000125378
GATACCTGAGACGGGGAAGAAAAAAGTCGCCGAGATTCAGGG-CCACGCGG
BMP4 KO
guide 1
GATACCTGA-ACGGGGAAGAAAAAAGTCGCCGAGATTCAGGG-CCACGCGG
BMP4 KO
guide 2
GATACCTGAGACGGGGAAGAAAAAAGTCGCCGAGATTCAGGGCCCACGCGG
E
BMP4 mRNA
(fold change)
1.00
0.75
0.50
0.25
0.00
WT
BMP4-KO g1
BMP4-KO g2

Supplemental Figure 1 (Related to STAR* Methods): Validation of culture platform and cell lines.

(A) WT-RUES2 cultured as a confluent, pseudostratified, polarized epithelium. Cells were seeded with a starting seeding density of ~4,000 cells/mm^2. 24 hrs after seeding, cells were fixed and stained for markers of tight junctions (ZO-1) and actin (Phalloidin). Scale bars = 50 μm. (B) Sequence integrity of our engineered TRE::BMP4-myc and TRE::NOGGIN-V5 cell lines showing the location of the Myc and V5 tags. (C) G-band karyotyping results of our engineered hESC lines show normal human female karyotypes. (D) Generation of two BMP4-KO hESC lines: Genomic sequencing demonstrates the location of the deletion (BMP4-KO guide 1) and insertion (BMP4-KO guide 2) point mutations at exon 3 of the BMP4 gene as a result of CRSPR/Cas9-mediated non-homologous end joining. (E) qPCR quantification of BMP4 mRNA in the BMP4-KO lines suggests homogeneous BMP4 knockout has occurred in both BMP4-KO lines. n = 3. Error bars = SD.

SF2

A

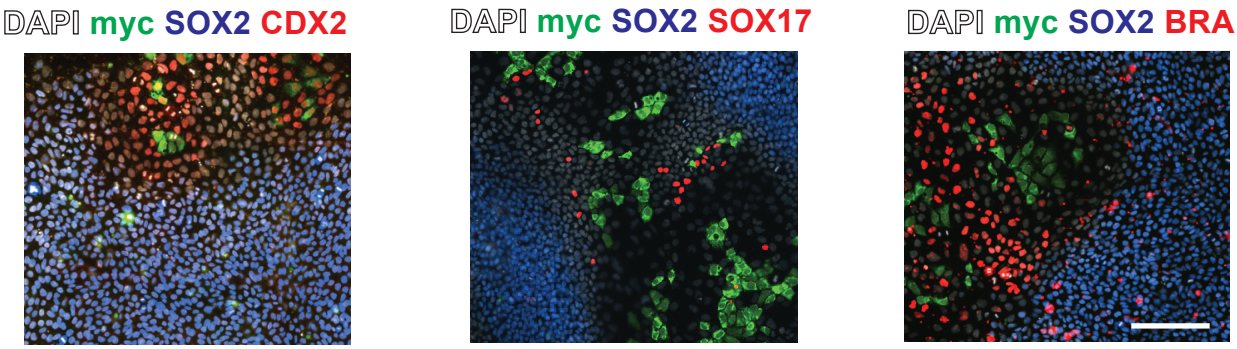
DAPI myc SOX2 CDX2
DAPI myc SOX2 SOX17
DAPI myc SOX2 BRA

B

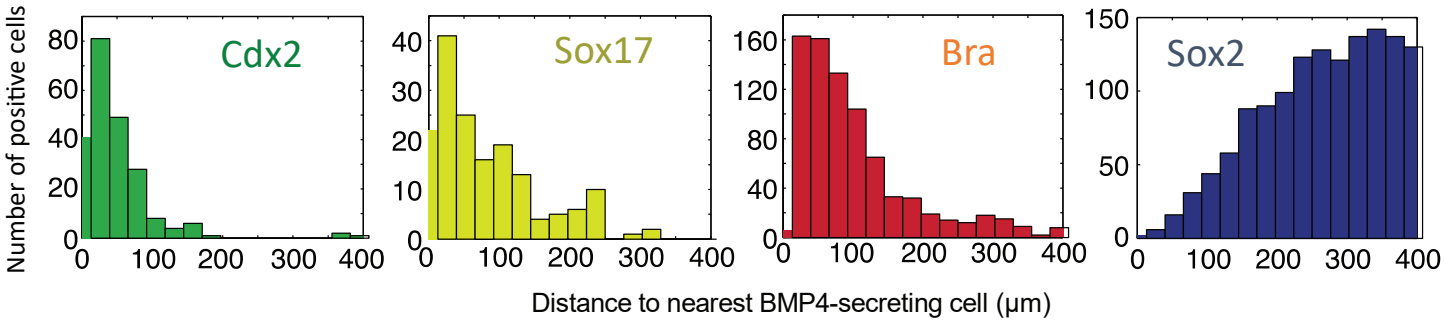
Number of positive cells
Cdx2
Sox17
Bra
Sox2
Distance to nearest BMP4-secreting cell (μm)

C

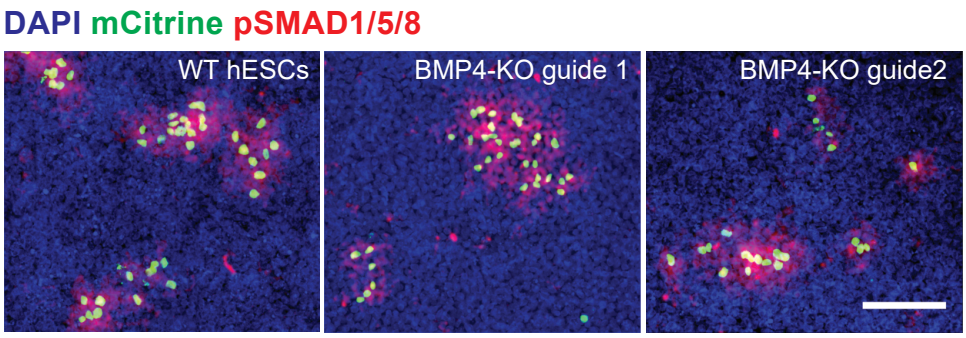
DAPI mCitrine pSMAD1/5/8
WT hESCs
BMP4-KO guide 1
BMP4-KO guide2

D

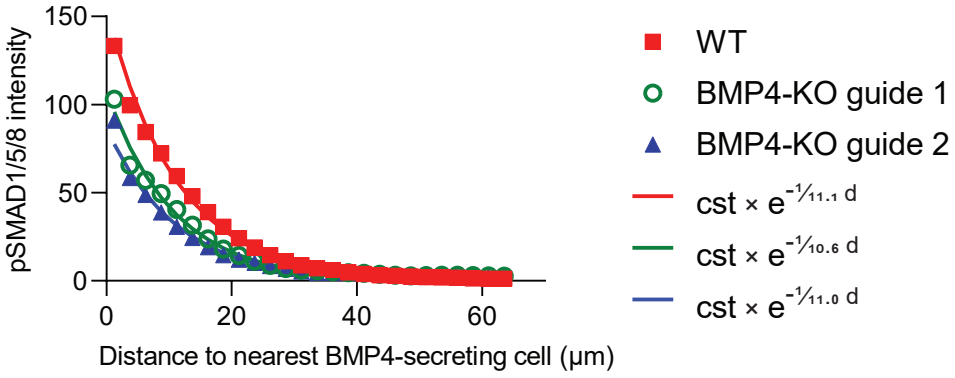
pSMAD1/5/8 intensity
Distance to nearest BMP4-secreting cell (μm)
WT
BMP4-KO guide 1
BMP4-KO guide 2
cst × e^-1/11.1 d
cst × e^-1/10.6 d
cst × e^-1/11.0 d

Supplemental Figure 2 (Related to Figure 1): Signaling dynamics associated with BMP4-secreting cells.

(A) BMP4-secreting cells induce the expected pattern of germ layer markers. TRE::xBMP4-myc cells were co-cultured with WT hESCs on glass surface. TRE::xBMP4-myc cells were induced with 0.2 μg ml^{-1} doxycycline to produce BMP4. The cells were stained for embryonic germ layer markers (SOX2 = epiblast/ectodermal fate; BRA = mesodermal fate; SOX17 = definitive endodermal fate; CDX2 = extraembryonic fate). Scale bars = 100 μm. (B) Quantification of embryonic germ layer markers as a function of distance from the nearest TRE::xBMP4-myc cell. (C) pSMAD1/5/8 signaling propagation was similar in WT and BMP4-KO hESCs. TRE::xBMP4-myc; CAG::H2B-mCitrine cells were co-cultured with WT hESCs or BMP4-KO hESCs on filters. Doxycycline was added for 12 hrs. (D) Quantification of BMP4 signal propagation as a function of distance to the nearest BMP4-secreting cells. There was no significant difference between the range of pSMAD1/5/8 activation in BMP4-KO hESCs and WT hESCs. Exponential curves were fitted to the datapoints. The exponential function is described by the constant "cst" which is the prefactor of the exponent function and the spreading length (in μm) which characterizes the function's rate of decay. Error bars = SEM.

SF3

A

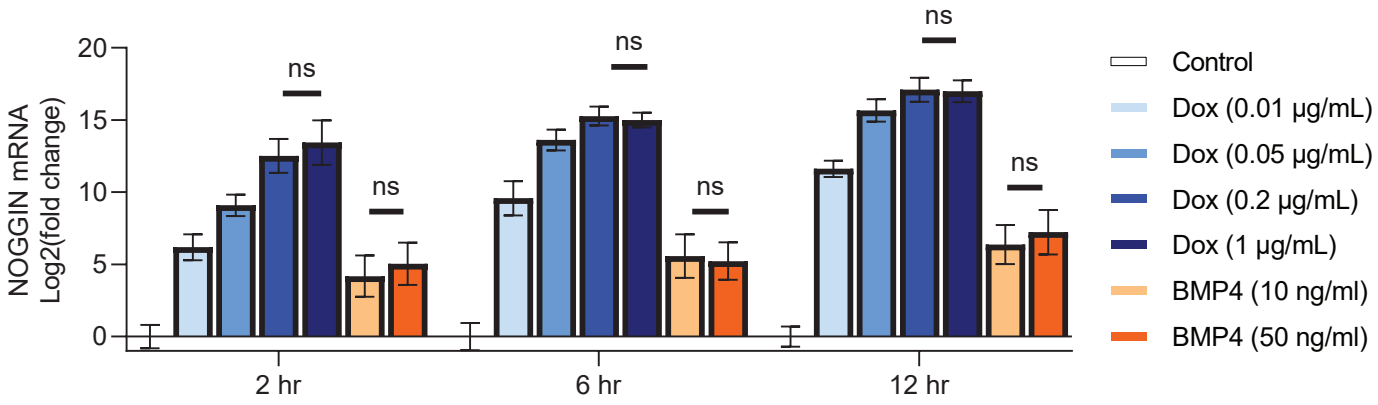
NOGGIN mRNA
Log2(fold change)
20
15
10
5
0
ns
ns
ns
ns
ns
ns
2 hr
6 hr
12 hr
Control
Dox (0.01 µg/mL)
Dox (0.05 µg/mL)
Dox (0.2 µg/mL)
Dox (1 µg/mL)
BMP4 (10 ng/ml)
BMP4 (50 ng/ml)

B

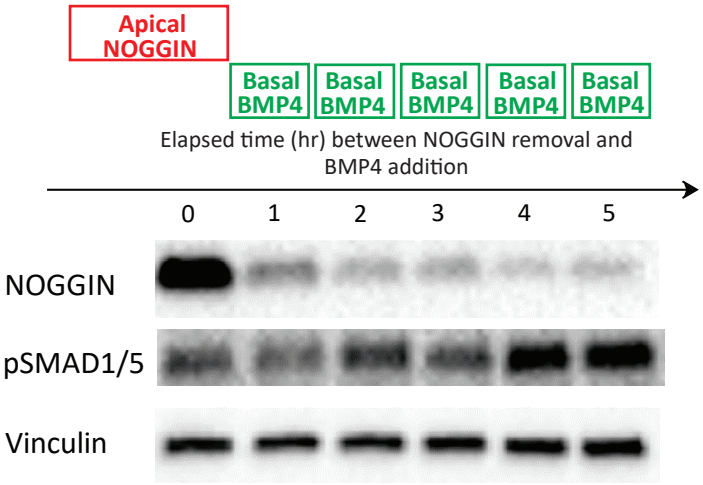
Apical NOGGIN
Basal BMP4
Basal BMP4
Basal BMP4
Basal BMP4
Basal BMP4
Elapsed time (hr) between NOGGIN removal and BMP4 addition
0
1
2
3
4
5
NOGGIN
pSMAD1/5
Vinculin

C

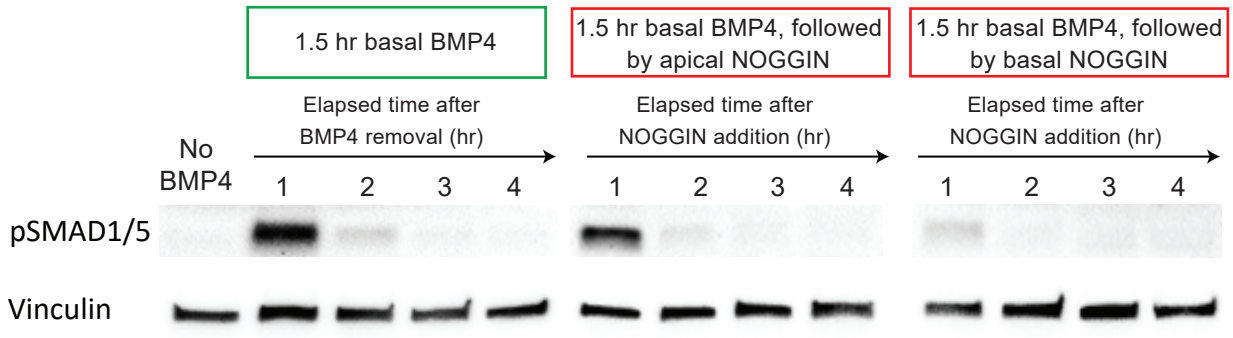
1.5 hr basal BMP4
1.5 hr basal BMP4, followed by apical NOGGIN
1.5 hr basal BMP4, followed by basal NOGGIN
Elapsed time after BMP4 removal (hr)
Elapsed time after NOGGIN addition (hr)
Elapsed time after NOGGIN addition (hr)
No BMP4
1
2
3
4
1
2
3
4
1
2
3
4
pSMAD1/5
Vinculin

Supplemental Figure 3 (Related to Figures 2 and 3): Dynamics of apical NOGGIN inhibition as shown by Western blot of hESC lysates.

(A) Comparison of NOGGIN mRNA levels induced by Dox relative to normal physiological levels induced by BMP4. TRE::NOGGIN-V5 hESCs were cultured on filters and induced with varying concentrations of doxycycline or with recombinant BMP4. After indicated amounts of induction time, cells were collected for qPCR quantifying levels of NOGGIN mRNA. The level of NOGGIN mRNA produced was saturated at 0.2 μg ml^{-1} Doxycycline. All groups were significantly different from the "Control" group. n = 3. Error bars = SD. (B) NOGGIN inhibitory effect on pSMAD1/5/8 was maintained for up to 3 hours after NOGGIN washout. Pre-treatment of hESCs with apical NOGGIN for (250 ng ml^{-1}; 2 hr) was followed by different time intervals before basal BMP4 (10 ng ml^{-1}; 1 hr) was added. The interval between each addition of BMP4 increased by 1 hr with each iteration. (C) pSMAD1/5/8 induced by basally-applied recombinant BMP4 was inhibited by apically- and basally-applied recombinant NOGGIN. WT hESCs were induced by a 1.5-hr pulse of BMP4 (10 ng ml^{-1}). Subsequently, BMP4 was washed out and simultaneously NOGGIN (250 ng ml^{-1}) was applied apically or basally for 2 hr. Cell lysates were collected to analyze with Western blot. (The first experiment in (C) is a control with no added NOGGIN).

SF4

A

Top view

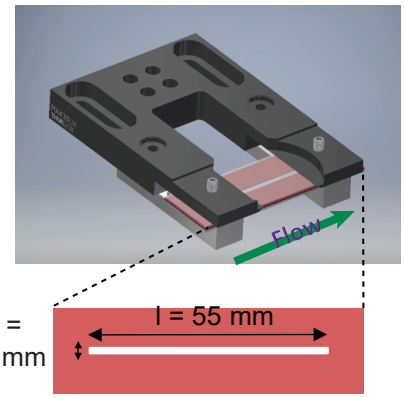

B

Side view

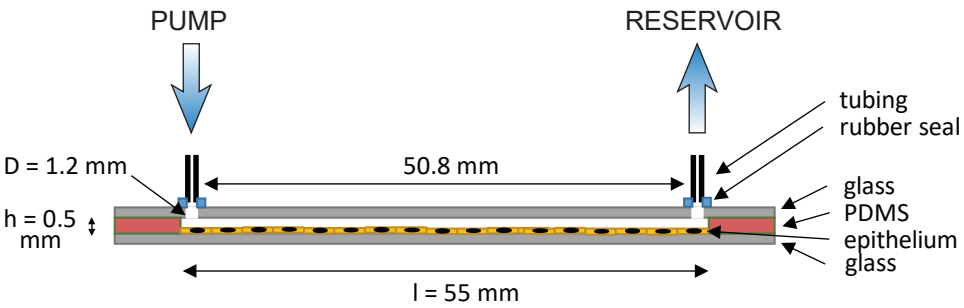

C

$$Re = \frac{Q \cdot D_H}{\nu \cdot A}$$

$Q_{low\ flow} = 10\ \mu l\ h^{-1} = 0.00278\ mm^3\ s^{-1}$
$Q_{high\ flow} = 1000\ \mu l\ h^{-1} = 0.278\ mm^3\ s^{-1}$

$$D_H = \frac{4 \cdot w \cdot h}{2(w+h)} = \frac{4 \cdot 2\ mm \cdot 0.5\ mm}{2(2\ mm + 0.5\ mm)} = 0.8\ mm$$

$\nu_{water,\ 37oC} = 0.6959\ mm^2\ s^{-1}$
$A = w \cdot h = 2\ mm \cdot 0.5\ mm = 1\ mm^2$

$$Re_{low\ flow} = \frac{Q \cdot D_H}{\nu \cdot A} = \frac{0.00278\ mm^3\ s^{-1} \cdot 0.8\ mm}{0.6959\ mm^2\ s^{-1} \cdot 1\ mm^2} = 0.00320$$

$$Re_{high\ flow} = \frac{Q \cdot D_H}{\nu \cdot A} = \frac{0.278\ mm^3\ s^{-1} \cdot 0.8\ mm}{0.6959\ mm^2\ s^{-1} \cdot 1\ mm^2} = 0.320$$

D

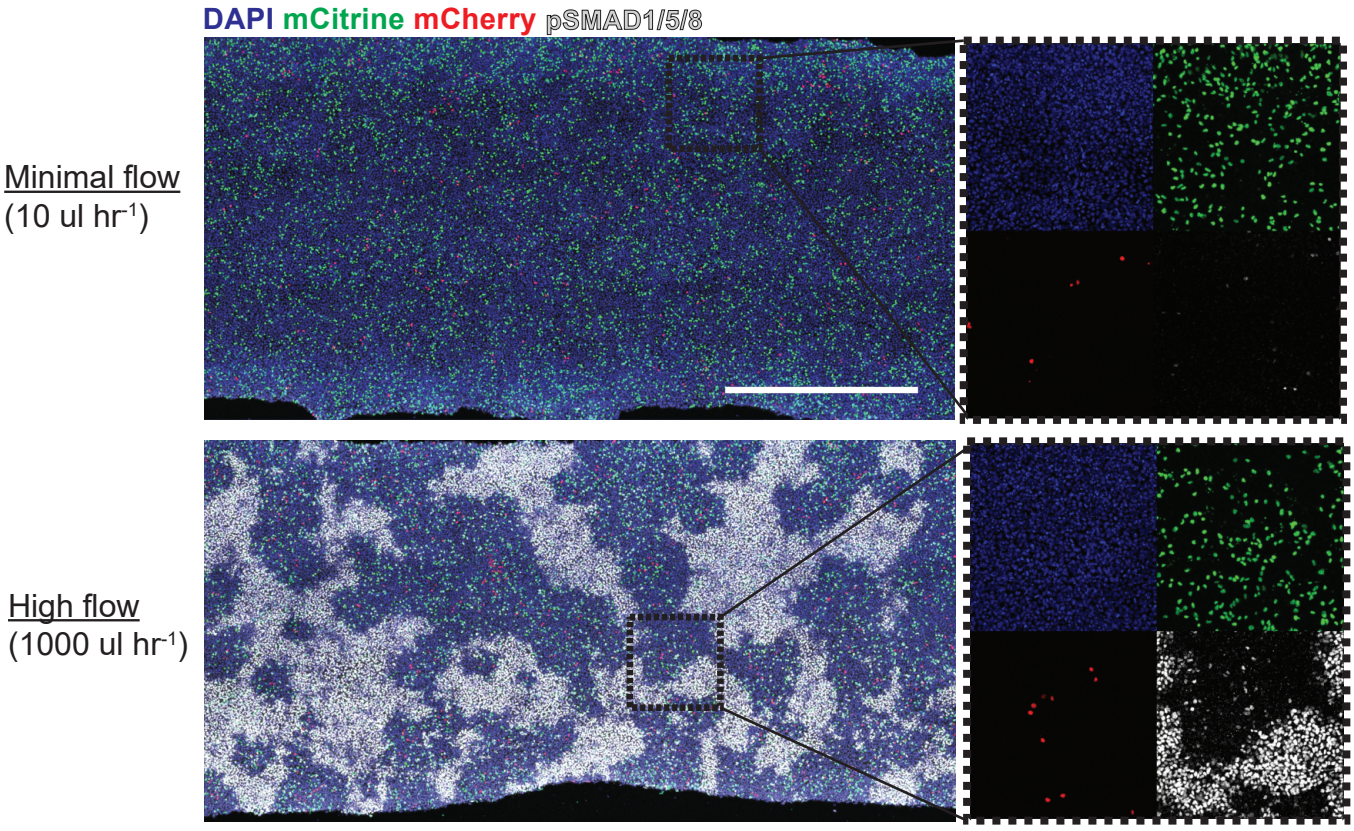

Supplemental Figure 4 (Related to Figure 4): Schematics of microfluidic device.
A PDMS layer (red), cast from a custom 3D-printed mold, was sandwiched between two glass slides to form a tightly-sealed chamber. Chamber dimensions were 55 mm x 2 mm x 0.5 mm. The top slide had drilled inlet and outlet holes. The culture chamber and tubing were securely fastened by a custom clamping device. (A) Top view. (B) Side view. (C) The calculated Reynold's numbers for the two flow conditions showed that the flow inside the chamber was laminar. (D) The epithelium within the microfluidic chamber corresponding to the data shown in Figure 4D. A wider view of the epithelium showed the differences in pSMAD1/5/8 response as related to different patterns of distribution of and degrees of proximity to the TRE::xBMP4-myc; CAG::H2B-mCitrine and TRE::hNOGGIN-V5; CAG::H2B-mCherry. Scale bar = 1000 μm.

SF5

A

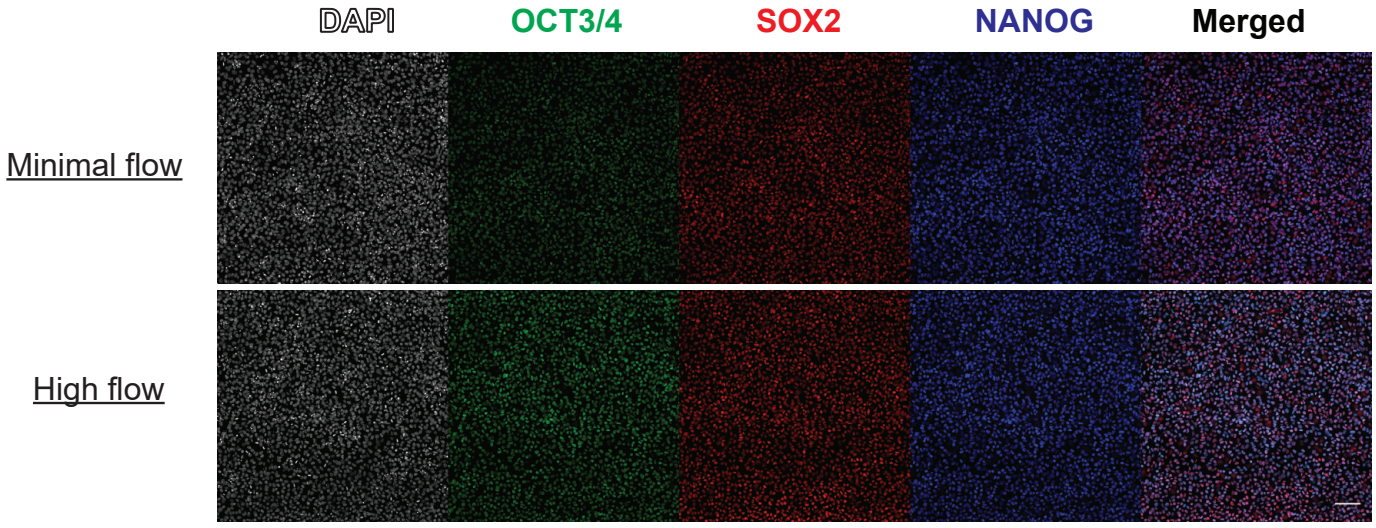
DAPI
OCT3/4
SOX2
NANOG
Merged
Minimal flow
High flow

B

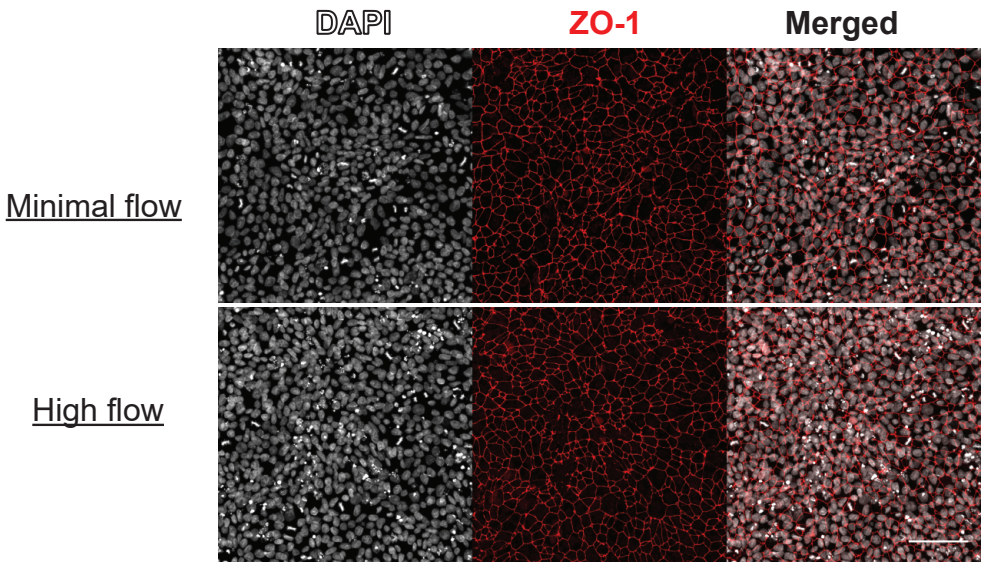
DAPI
ZO-1
Merged
Minimal flow
High flow

C

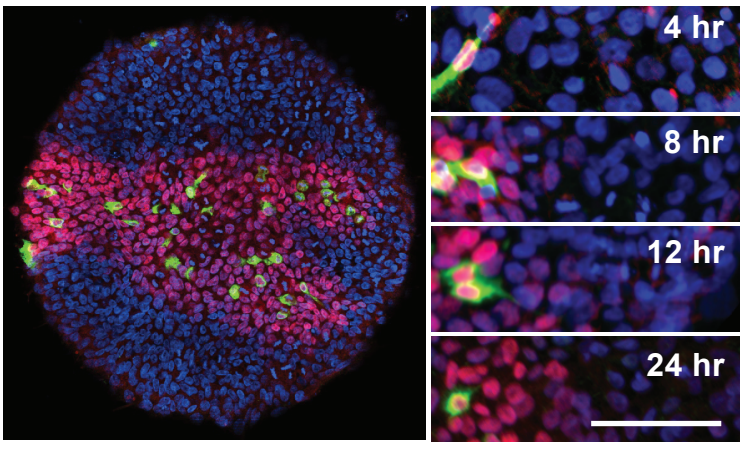
DAPI BMP4 pSMAD1/5
4 hr
8 hr
12 hr
24 hr

D

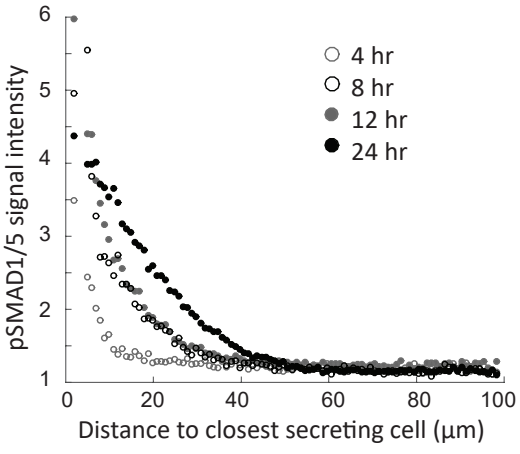
pSMAD1/5 signal intensity
Distance to closest secreting cell (µm)
4 hr
8 hr
12 hr
24 hr
1
2
3
4
5
6
0
20
40
60
80
100

E

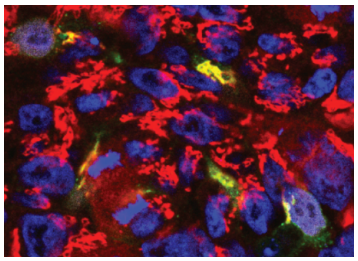
DAPI
V5
GIANTIN

Supplemental Figure 5 (Related to Figure 4): Validation of the cell culture condition within the microfluidic device.

(A) hESCs maintained pluripotency under minimal flow in microfluidic culture. After hESCs were cultured on glass-bottomed microfluidic chamber under minimal flow (10 μl hr^{-1}) overnight, the flow rate was increased to 1000 μl hr^{-1} (High flow) for 9 hr. Cells in the microfluidic chamber were stained for pluripotency markers OCT3/4, SOX2, and NANOG. (B) Cells were also stained for tight junction markers ZO-1. (C) BMP4 signaling propagated on glass substrate. TRE::xBMP4-myc cells were co-cultured with WT hESCs (ratio 1:200) on glass micropatterned chip. The cells were induced to produce BMP4 for the specified durations. pSMAD1/5/8 immunolabeling defined the range of BMP4 signaling. Scale bars = 100 μm. (D) Quantification of BMP4 signaling propagation as a function of time on glass substrates. The rate of spreading was comparable to cells on filters in Fig 1E. (E) Intense V5 labeling overlapping with Golgi marker GIANTIN (Linstedt & Hauri, 1993) indicated TRE::hNOGGIN-V5 cells.

A

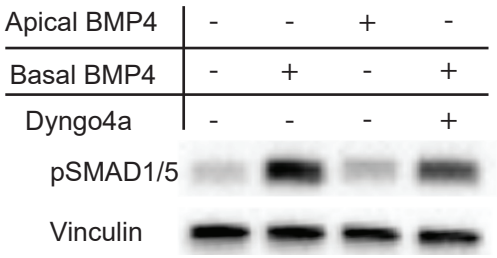
Apical BMP4 - - + -
Basal BMP4 - + - +
Dyngo4a - - - +
pSMAD1/5
Vinculin

B

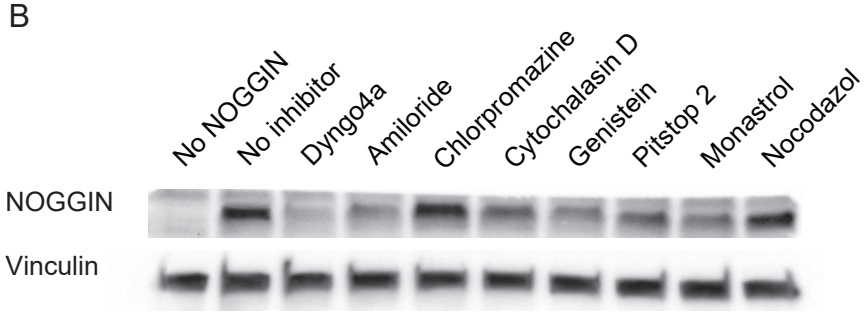
No NOGGIN
No inhibitor
Dyngo4a
Amiloride
Chlorpromazine
Cytochalasin D
Genistein
Pitstop 2
Monastrol
Nocodazol
NOGGIN
Vinculin

C

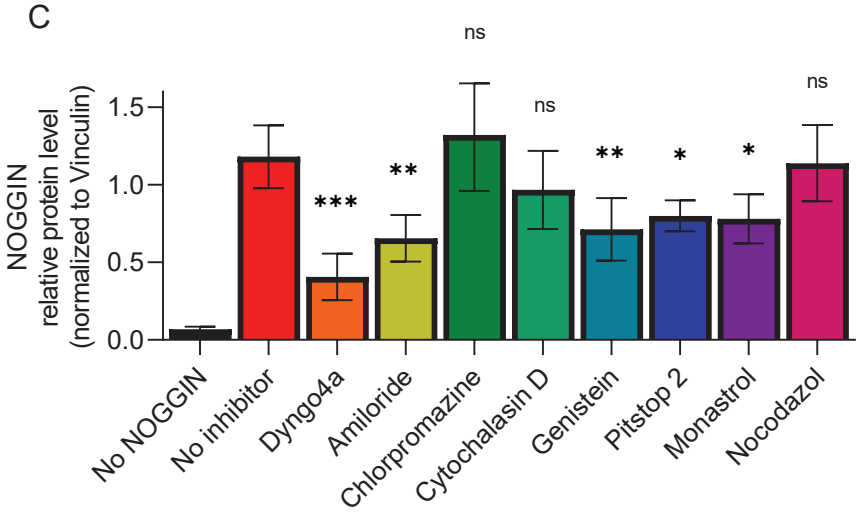
NOGGIN relative protein level (normalized to Vinculin)
1.5
1.0
0.5
0.0
ns
***
**
ns
**
*
*
ns
No NOGGIN
No inhibitor
Dyngo4a
Amiloride
Chlorpromazine
Cytochalasin D
Genistein
Pitstop 2
Monastrol
Nocodazol

D

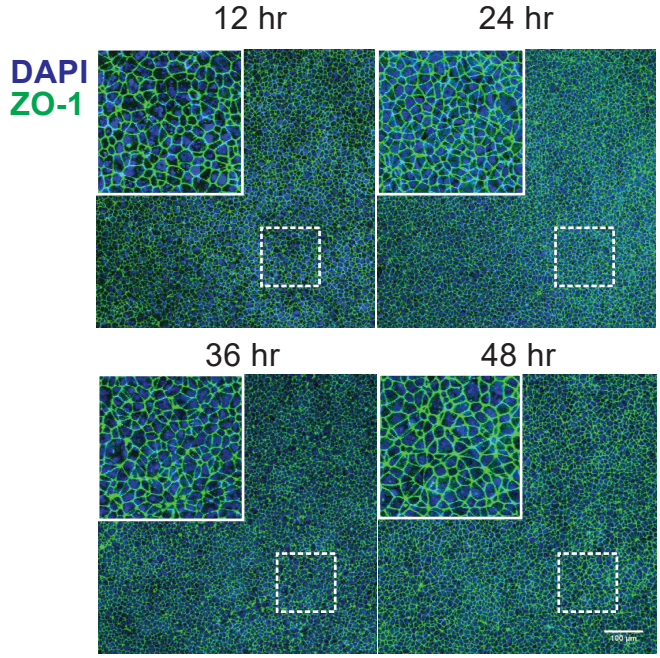
12 hr
24 hr
DAPI
ZO-1
36 hr
48 hr

E

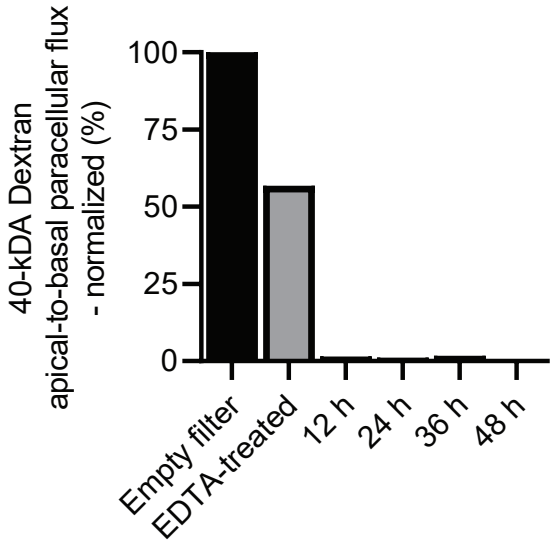
40-kDA Dextran apical-to-basal paracellular flux - normalized (%)
100
75
50
25
0
Empty filter
EDTA-treated
12 h
24 h
36 h
48 h

F

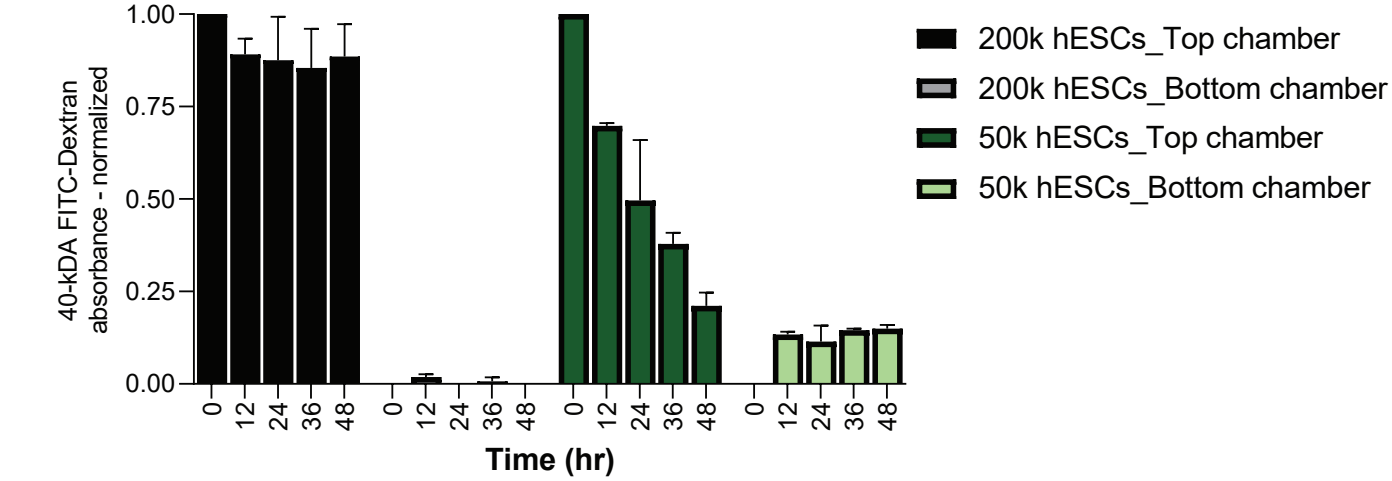
40-kDA FITC-Dextran absorbance - normalized
1.00
0.75
0.50
0.25
0.00
0
12
24
36
48
Time (hr)
200k hESCs_Top chamber
200k hESCs_Bottom chamber
50k hESCs_Top chamber
50k hESCs_Bottom chamber

Supplemental Figure 6 (Related to Figure 6): Effect of different pharmacological inhibitors on NOGGIN internalization and Validation of epithelial integrity

(A) Dynamin-dependent endocytosis of BMP4 was not required for BMP4 signaling WT hESCs were stimulated with BMP4 (50 ng ml^{-1}; 30 min) with or without 30-min pre-treatment of Dyngo4a (100 mM) The drug did not affect the response to basal BMP4. Cell lysates were collected for Western blot analysis. (B) NOGGIN internalization was inhibited by different endocytosis inhibitors. WT hESCs were cultured on transwell filters. Recombinant NOGGIN (250 ng ml^{-1}) was added to the apical compartment. Each inhibitor was also added to the apical compartment. A detailed description of the concentration used for each inhibitors and the effects of each inhibitor can be found in Supplementary Table 1. After 2 hrs, the cell lysates were collected for Western blotting. (C) Quantification of the effects of different endocytosis inhibitors on NOGGIN internalization. Error bars = SD. Dunnett's multiple comparison statistical tests were performed with n = 3 (ns = not significant; * $p \leq 0.05$; ** $p \leq 0.01$; *** $p \leq 0.001$). (D) Cells maintained normal ZO-1 expression following transcytosis experiment. Following transcytosis experiment in Figure 6E, the same epithelia were evaluated for expression pattern of tight junction marker ZO-1. All epithelia examined showed an intact mesh of ZO-1. Scale bar = 100 μm. (E) Epithelia were impermeable to 40-kDA dextran after the transcytosis experiment. Following transcytosis experiment in Figure 6E, the same epithelia was evaluated for epithelial permeability at the corresponding times. 40-kDA dextran-TxRed (25 mg/ml) was added to the apical chamber, for 1 hour (37°C, 5% CO2), with or without a pre-treatment of chelating agent EDTA (50 mM, 30 min). Fluorescence intensity in the basolateral compartment was measured by a fluorometer (NanoDrop 2000), set at an absorbance of 589 nm. Epithelial permeability was assessed by measuring the TxRed-labeled dextran flux from the apical to the basolateral chambers. (F) Epithelium integrity was maintained during 48 hrs filter culture. We compared the permeability of epithelia seeded with 200,000 hESCs (standard culture condition used throughout this study) and epithelia seeded with 50,000 hESCs (low cell density condition). While the epithelia prepared with standard protocol demonstrated impermeability, the epithelia seeded with less cells demonstrated leakiness: 40-kDA Dextran-FITC added to the top media was found in the basal media in the latter condition but not the first.

Supplementary Table 1 (Related to STAR* Methods):
List of pharmacological inhibitors used and their reported effects on endocytosis.

Inhibitor	Concentration	Effect(s)	Internalization pathway(s) affected	References
Dyngo4a	100 uM	Dynamin inhibition	Clathrin-dependent endocytosis	Park et al., 2013 McCluskey et al., 2013
Amiloride	100 uM	Sodium-proton exchanger inhibition Actin disruption	Macropinocytosis	Delvaux et al., 1990 Lagana et al., 2000 Koivusalo et al., 2010 Dutta and Donaldson, 2012
Chlorpromazine	100 uM	Clathrin inhibition	Clathrin-dependent endocytosis	Wang et al., 1993
Cytochalasin D	10 uM	Actin depolymerization	Clathrin-dependent endocytosis Macropinocytosis	Schliwa, 1982 Sampath and Pollard, 1991 Jackman et al., 1994 Fujimoto et al., 2000
Genistein	100 uM	Tyrosine kinase inhibition Actin disruption Dynamin inhibition	Caveolae-dependent endocytosis	Akiyama et al., 1987 Aoki et al., 1999 Nabi and Le, 2003
Pitstop 2	33 uM	Clathrin inhibition	Clathrin-dependent endocytosis Clathrin-independent endocytosis	von Kleist et al., 2011 Dutta et al., 2012 Willox et al., 2014
Monastrol	100 uM	Kinesin inhibition Calcium-channel inhibition	Clathrin-dependent endocytosis	Mayer et al., 1999 Harasztosi et al., 2018 Witte et al., 2020 Abassi et al., 2009 Huang et al., 2017 Yao et al., 2017
Nocodazol	16.6 uM	Microtubule disruption	Clathrin-dependent endocytosis	Hoebeke et al., 1976 Hamm-Alvarez et al., 1996 Vasquez et al., 1997 Subtil and Dautry-Varsat, 1997